A theoretical model of the explosive fragmentation of vesicular magma

A. C. Fowler,
MACSI, Department of Mathematics and Statistics,
University of Limerick, Limerick, Republic of Ireland.

Bettina Scheu,
Earth and Environmental Sciences, LMU München,
Theresienstrasse 41/111, 80333 München, Germany.

W. T. Lee,
MACSI, Department of Mathematics and Statistics,
University of Limerick, Limerick, Republic of Ireland.

M. J. McGuinness
School of Mathematics, Statistics and Operations Research,
Victoria University of Wellington, New Zealand.

October 6, 2009

Abstract

Recent experimental work has shown that when a vertical column of rock under large pressure is suddenly depressurised, the column can 'explode' in a structured and repeatable way. The observations show that a sequence of horizontal fractures forms from the top down, and the resulting blocks are lifted off and ejected. The blocks can suffer secondary internal fractures. This experiment provides a framework for understanding the way in which catastrophic explosion can occur, and is motivated by the corresponding phenomenon of magmatic explosion during Vulcanian eruptions. We build a theoretical model to describe these results, and show that it is capable of describing both the primary sequence of fracturing, and the secondary intra-block fracturing. The model allows us to suggest a practical criterion for when such explosions occur: firstly, the initial confining pressure must exceed the yield stress of the rock, and secondly, the diffusion of the gas by porous flow must be sufficiently slow that a large excess pore pressure is built up. This will be the case if the rock permeability is small enough.

Keywords: Magma fragmentation, brittle fragmentation, silicic magma, explosive volcanism.

1 Introduction

Depending on magma composition and evolution, explosive volcanic eruptions manifest themselves in a broad variety of activity ranging from mild Strombolian eruptions and Hawaiian fire fountaining to vigorous Vulcanian and Plinian eruptions. The range of different types of explosive eruption is mirrored in the variety of their trigger mechanisms. Vulcanian-style eruptions are typically caused by the sudden unplugging of a sealed volcanic vent. The consequent depressurisation of the underlying magma generates stresses in the vesicular magma and may initiate further volatile exsolution; if the magma is sufficiently viscous, the gases are not able to escape from the pressurised vesicles, thus adding further stress to the magma which can cause brittle rupture of the magma itself, resulting in an explosive eruption.

It is this fragmentation of magma which distinguishes explosive volcanic eruptions from the more quiet effusive form of volcanic activity. Hence the conditions leading to magma fragmentation as well as the fragmentation process itself are key points for the understanding of the dynamics of volcanic eruptions. So far various models have been proposed for fragmentation, based on investigations of deposits of explosive eruptions, theoretical models and laboratory experiments. Early models mentioned magma disruption by bubble coalescence as the main mechanism (Verhoogen 1951). However, McBirney and Murase (1970) and Sparks (1978) demonstrated that coalescence is unlikely to be the leading fragmentation mechanism for highly viscous magmas, although possibly applicable for eruptions of low viscosity magmas. Basically two main groups of processes leading to fragmentation can be discriminated:

1. Fragmentation due to rapidly accelerating two phase flow.

In this case the driving force for expansion and acceleration is derived from vesiculation and bubble growth. High strain rates within the magma cause the fragmentation, either due to instabilities in the fluid (ductile) or by brittle fracture. Low viscosity magma is likely to fragment by fluid instabilities resulting in Hawaiian fire fountains or Strombolian bubble bursts. Fragmentation by brittle fracture due to high strain rates may be important for Plinian eruptions of higher viscous magma (Dingwell and Webb 1989, Gilbert and Sparks 1998, Papale *et al.* 1998, Papale 1999, Cashman *et al.* 2000).

2. Fragmentation of vesicular magma due to rapid decompression.

Here, gas overpressure builds up in the vesicles of the magma, mainly depending on melt properties as viscosity, volatile content, and diffusivity as well as the overburden pressure. Rapid decompression of the vesicular magma can be triggered by the sudden removal of an edifice (e. g., dome collapse or landslide) or by ejection of a plug from the conduit. A pressure gradient is built up at top of the magma body between the pressurized gas in the vesicles and the low pressure area behind the unloading wave. At a certain pressure differential, the tensile strength of the magma is overcome and

brittle disruption of the upper layer within the vesicular magma will occur. Now a newly formed free surface is exposed to low pressures and again a pressure gradient is built up, leading to the fragmentation of the next layer. Thus, a layer by layer fragmentation process (a fragmentation wave) moves downwards into the magma (Alidibirov and Dingwell 1996, 2000, Scheu *et al.* 2008). Calculations demonstrate that the fragmentation wave velocity should be far slower than the speed of sound. This was confirmed subsequently experimentally, with values ranging from 2 to 110 m s^{-1} (Kennedy *et al.* 2005, Scheu *et al.* 2006). This fragmentation process plausibly accounts for the eruption style of most silicic events, e. g., for lateral blasts and Vulcanian to sub-Plinian eruptions. It may further contribute to Plinian eruptions of silicic magma, most likely in combination with the other mechanism mentioned above.

Layer by layer fragmentation is nowadays widely accepted as being the predominant fracturing process caused by rapid decompression (Cashman *et al.* 2000, Melnik 2000, Ichihara *et al.* 2002, Namiki and Manga 2005, Scheu *et al.* 2006, Scheu *et al.* 2008).

Several physical models have been proposed accounting for the stress distribution caused by pressurized gas within the vesicles of a magma body. McBirney and Murase (1970) used elasticity theory and the Griffith theory of fracture. More recent models are based on the stress distribution of thin-walled spheres (Alidibirov 1994) or thick-walled spheres (Zhang 1999). Based on laboratory experiments, Spieler *et al.* (2004) linked overpressure and porosity in an empirical fragmentation criterion. Comparative studies of these models, including comparisons to experimental data sets, showed that none of the approaches fit the entire range of data accurately enough, leading to the suggestion that the process is intrinsically more complex (Spieler *et al.* 2004, Koyaguchi *et al.* 2008). Koyaguchi *et al.* (2008) added the Griffith theory of crack propagation to the models of Zhang (1999) and Koyaguchi and Mitani (2005), and thus was able to reproduce satisfactorily not only the threshold for magma fragmentation, but also its propagation speed (Scheu *et al.* 2006).

Our aim in this paper is to describe a mathematical model based on first principles of mass and momentum conservation which can explain the experimental results. In principle, this will provide a theoretical framework for the subsequent investigation of the more realistic situation which occurs in an actual volcanic vent. The experimental setup is described in the following section.

2 Experimental investigations

Experimental setup

To investigate the fragmentation of porous magma induced by rapid decompression, Alidibirov *et al.* (1994) designed a vertical shock tube apparatus. This was improved and modified several times to suit different scientific problems (Spieler *et al.* 2004, Scheu *et al.* 2006, 2008a,b), yet the basic principle remains the same: a cylindrical sample (in this study 12 mm radius and 60 mm length) of a porous volcanic rock is

glued into a sample holder and placed in an autoclave. A set of diaphragms separates the autoclave from a large chamber at atmospheric pressure. The autoclave with the sample inside is slowly pressurized with nitrogen gas. After an equilibration time, rapid decompression is triggered by a systematic failure of the diaphragm system. When the rarefaction wave reaches the sample a pressure gradient starts to build up in the sample leading to disruption of the sample and ejection of the fragments (above the fragmentation threshold) or to permeable degassing of the entire sample (below the fragmentation threshold).

Figure 1 depicts the specific setup used for this study, which was optimized for visual observation (Scheu *et al.* 2008a). The autoclave as well as the sample holder were manufactured out of plexiglass, and all experiments were performed at ambient temperature. Special care was taken to use a transparent glue neither obscuring the view nor changing the appearance of the sample. Three pressure sensors monitor the gas pressure evolution within the autoclave (above the sample), at the side of the sample as well as directly below it. A high speed video camera (Photron Fastcam) records the experiment at a rate of 10,000 frames per second.

In these experiments magma is represented by a sample of porous volcanic rock. The use of rock to represent magma can be justified by the rapidity of the decompression. On the millisecond timescale of these experiments, magma behaves like a brittle solid rather than a viscous liquid (Dingwell 1996). When the autoclave is decompressed the sample remains pressurized for a certain time due to the gas in its open pore space, causing it to fragment.

Experimental results

In a series of experiments, different glues were tested to ensure optimal experimental conditions. The chosen glue, a special superglue, does not penetrate into the sample and is applied to the entire inner surface of the sample holder. The glue is brittle and only just strong enough to hold the sample in place against the pressure difference developed between its top and bottom when the autoclave is decompressed. If no glue is used, the entire sample is propelled upwards by compressed gas ejected from its base but shows a similar pattern of fractures. If the glue holds the sample in place too strongly, the sample fractures internally leaving a shell of rock attached to the sleeve. In both these cases it is more difficult to observe the fracture pattern developing.

Figure 2 shows snapshots of a fragmenting sample recorded by a high speed camera at 10,000 frames per second. These indicate that fragmentation starts at the top of the sample and continues downwards. Two types of fractures are observed. The first type is fracture of the glued column, and usually occurs within the upper third of the sample. The fractures are parallel to the sample surface and dissect the entire sample into discs (layers). Crystals, large pores and preexisting small cracks may cause a slight deviation from this fracture pattern. The second type is internal fracturing of an expelled fragment. After a disc is ejected, further fracturing may be observed during ejection. This consecutive fracturing often leads to an entire disaggregation of the sample into ash and small blocky fragments.

A more complicated picture of the second type of fracture is revealed by figure

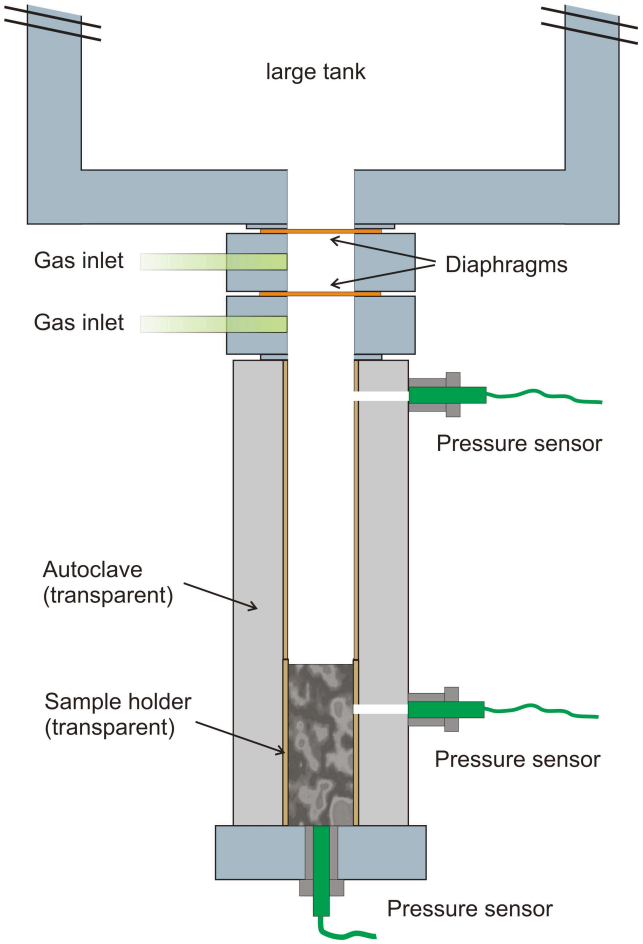

Figure 1: Shock tube based apparatus for magma fragmentation. The sample is glued to a holder, placed inside the autoclave and slowly pressurized using nitrogen gas. The autoclave is decompressed by opening the diaphragms at the top. Pressure sensors measure the resulting decline of gas pressure with time, while a high speed video camera captures the sequential fracturing of the rock.

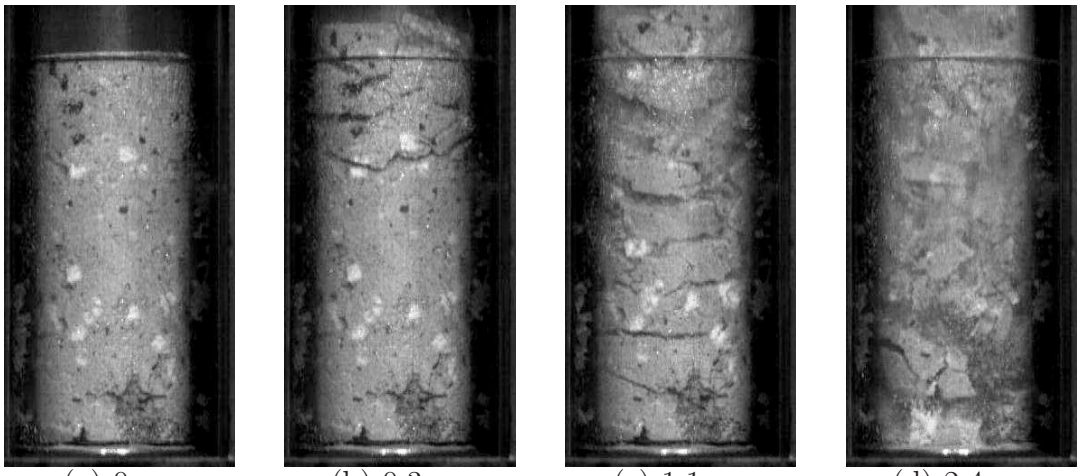

(a) 0 ms (b) 0.3 ms (c) 1.1 ms (d) 2.4 ms

Figure 2: Individual frames from a movie taken by a high speed digital camera during a typical rock fragmentation experiment. (a) Before depressurization of the autoclave has taken place. (b) 0.3 ms after decompression commenced, the upper part of the sample has fractured. (c) After 1.1 ms fractures have occurred throughout the sample. (d) By 2.4 ms the rock has disintegrated.

3, which gives the locations of the upper and lower surfaces of cracks as a function of time. Slices of rock are ejected from the upper part of the remaining sample, but these slices can break into two or more discs, exhibiting layered fractures while in flight before they shatter into small pieces. This fracturing behaviour was systematically observed in the higher pressure experiments, and cannot be explained by the existing models of layer-by-layer fragmentation previously mentioned. Thus a comprehensive mathematical model of this process must be able to account for both these types of fracture.

3 A mathematical model of fragmentation

We consider the column of rock to be an elastic porous medium, and as such the basic theory for deformation of the medium is that given by Biot (1956, 1962). The gas can flow through the porous rock, and we suppose the rock fractures if the gas pore pressure exceeds the stress in the solid matrix by a yield stress σ_Y. When the pressure is lowered at the surface of the sample, the solid stress is lowered very rapidly, while a decompression wave propagates downwards through the pore space. It is the resulting excess pore pressure which can cause fracturing of the sample. In our theoretical discussion, we will describe the way in which sequential primary fracturing can occur, and also how secondary fracture within separated blocks can occur. A distinction that we will make is between experiments where the sample is glued to the container, and those where it is not. In the latter, we generally find (as is observed) that the column lifts off the base initially, before subsequently fracturing.

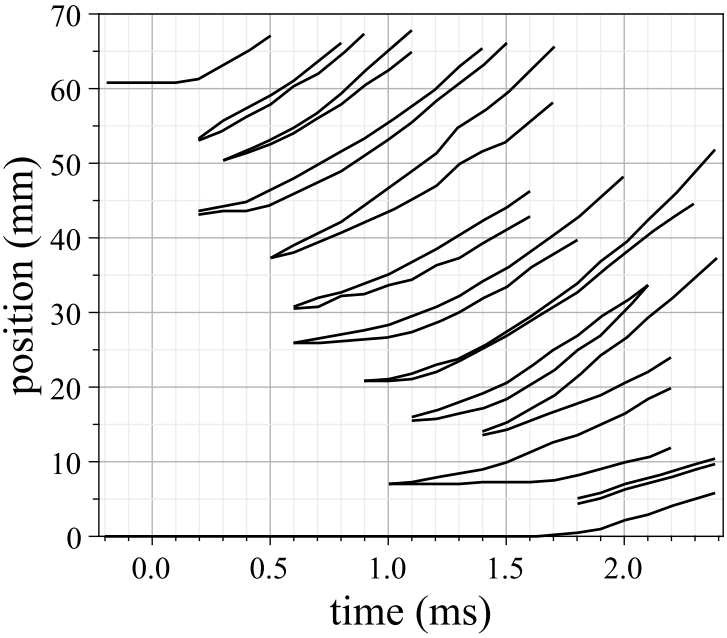

Figure 3: Graph showing the initiation and progress of cracks in a typical sample. (This is from the same experiment as that shown in figure 2.) The uppermost line shows the height of the top of the sample as a function of time; pairs of lines show the heights of the upper and lower surfaces of cracks; the lowermost line is the height of the base of the sample.

We interpret this as being due to a primary fracture at the base (where the yield stress is zero), followed by subsequent secondary fracture. If the sample is glued, then we suppose that a wall friction acts on the sample due to the glue, and this allows the possibility for primary internal fracturing. In the model which follows, we describe the elastic displacement of the rock and the turbulent porous flow of the (adiabatically compressible) gas through the rock, allowing for poroelastic effect of the gas pressure on the rock deformation.

In Biot's (1956) theory, the solid displacement is denoted $\mathbf{u}$, while the displacement of the pore fluid is denoted $\mathbf{U}$. The solid strain tensor is denoted e_{ij}, so that

$$e_{ij} = \frac{1}{2}\left(\frac{\partial u_i}{\partial x_j} + \frac{\partial u_j}{\partial x_i}\right), \tag{3.1}$$

and the dilatations of solid and fluid are defined by

$$e = e_{kk} = \boldsymbol{\nabla}.\,\mathbf{u}, \quad \varepsilon = \boldsymbol{\nabla}.\,\mathbf{U}. \tag{3.2}$$

Biot's equations for the stresses are then

$$\begin{aligned} (1-\phi)\sigma_{ij}^S &= 2Ne_{ij} + [Ae + Q\varepsilon]\delta_{ij}, \\ -\phi p &= Qe + R\varepsilon, \end{aligned} \tag{3.3}$$

where N, A, Q and R are four elastic constants; A and N are equivalent to Lamé constants for the solid matrix, and Q and R are associated with the deformability of the pore space and the pore fluid. Note that by eliminating ε, we can write $(3.3)_1$ in the form

$$(1-\phi)\sigma_{ij}^S = 2Ne_{ij} + [Be - \alpha p]\delta_{ij}, \tag{3.4}$$

where

$$B = A - \frac{Q^2}{R}, \quad \alpha = \frac{\phi Q}{R}. \tag{3.5}$$

(Biot writes the stress in the solid in the form $\sigma_{ij} = (1-\phi)\sigma_{ij}^S$.)

For small displacements, the velocity of the pore fluid is defined by

$$\mathbf{v} = \frac{\partial \mathbf{U}}{\partial t}. \tag{3.6}$$

Biot then poses conservation of momentum equations for the pore fluid and the matrix, which can be written in the form

$$\begin{aligned} \rho_f \phi \mathbf{v}_t &= -\phi \boldsymbol{\nabla} p - \mathbf{A} - \mathbf{D}, \\ \rho_s(1-\phi)\mathbf{u}_{tt} &= (1-\phi)\boldsymbol{\nabla}.\boldsymbol{\sigma}^S + \mathbf{A} + \mathbf{D}, \end{aligned} \tag{3.7}$$

where $\mathbf{A}$ and $\mathbf{D}$ are added mass and interfacial drag terms, taken by Biot in the form

$$\mathbf{A} = \rho_a \frac{\partial}{\partial t}(\mathbf{v} - \mathbf{u}_t), \quad \mathbf{D} = b(\mathbf{v} - \mathbf{u}_t). \tag{3.8}$$

The subscripts t denote time derivatives, here and subsequently. ρ_a is an added mass coefficient having units of density, and b is an interfacial drag coefficient. We discuss suitable forms for these coefficients below.

The model is completed by the addition of conservation of mass equations,

$$(\rho_f \phi)_t + \boldsymbol{\nabla}.(\rho_f \phi \mathbf{v}) = 0 \tag{3.9}$$

for the pore fluid, and

$$\{\rho_s(1-\phi)\}_t + \boldsymbol{\nabla}.\{\rho_s(1-\phi)\mathbf{u}_t\} = 0 \tag{3.10}$$

for the solid, together with an equation of state for the pore fluid, which in the present case we take to be the perfect gas law,

$$\rho_f = \frac{Mp}{RT}, \tag{3.11}$$

and an energy equation for the gas, which we take to be the adiabatic equation

$$\frac{dT}{dp} = \frac{1}{\rho_f c_p}, \tag{3.12}$$

where c_p is the specific heat at constant pressure.

The provenance of the conservation of mass of solid is a curiosity, since in the elastic description of the solid matrix, mass conservation is not generally considered. In fact the elastic description implicitly assumes small strains and essentially constant porosity, and we can interpret (3.10) as simply stating that ϕ is approximately constant. We shall thus not consider this equation further.

We now consider the specification of the coefficients ρ_a and b. The added mass coefficient commonly takes the form

$$\rho_a = \phi C_{VM} \rho_c \tag{3.13}$$

in dispersed two-phase flows (Robinson *et al.* 2008), where ϕ is the volume fraction of the dispersed phase, ρ_c is the density of the continuous phase, and C_{VM} is an $O(1)$ number. An example would be the bubbly flow of gas bubbles in a liquid phase, where ρ_c is the density of the liquid. The added mass force arises through the existence of relative motion between the phases. Because the liquid has to get round the gas bubbles, its corresponding deformation implies that $\rho_a \sim \rho_c$. In the present case, the relative motion of solid and pore gas is accommodated by deformation of the gas phase (both phases are continuous, i. e., connected), and therefore we suppose that ρ_a is given by

$$\rho_a = (1-\phi) C_{VM} \rho_f, \tag{3.14}$$

with $C_{VM} = O(1)$.

The drag coefficient b is most simply determined through analogy with Darcy's law. If we ignore the (usually small) acceleration terms in $(3.7)_2$, then (bearing in mind that the Darcy flux is $\phi\,(\mathbf{v} - \mathbf{u}_t)$), we see that Darcy's law is obtained by choosing

$$b = \frac{\eta_f \phi^2}{k} \tag{3.15}$$

(Biot 1956), where k is the permeability. In the present situation, the pore gas flow is sufficiently rapid that the Ergun equation may be appropriate. One form of this which caters for both Darcy (laminar) and Ergun (turbulent) forms is the Forchheimer equation

$$\boldsymbol{\nabla} p = \frac{\eta_f \mathbf{V}}{k} + \frac{\rho_f c_F |\mathbf{V}| \mathbf{V}}{\sqrt{k}} \tag{3.16}$$

(Nield and Bejan 2006), where in the present context $\mathbf{V} = \phi\,(\mathbf{v} - \mathbf{u}_t)$, and c_F is an $O(1)$ coefficient. The second term is dominant if the pore Reynolds number is large, i. e.,

$$\frac{\rho_f \sqrt{k} |\mathbf{V}|}{\eta_f} \gg 1, \tag{3.17}$$

and we anticipate that this is the case. It is then appropriate to define, equivalently to (3.16),

$$b = \frac{\eta_f \phi^2}{k} \left[1 + \frac{\rho_f c_F \sqrt{k}\,|\mathbf{V}|}{\eta_f} \right]. \tag{3.18}$$

One-dimensional model

Since the experimental results are in essence one-dimensional, we suppose that the variables depend only on the vertical coordinate z, where the initial sample lies in $0 < z < l$. The vertical solid displacement is denoted w, the vertical component of the solid stress σ^S_{33} is denoted σ, and the vertical velocity of the pore gas is denoted v. A complication arises depending on whether the sample is glued to, or otherwise pressed against, the sample holder. In this case it is appropriate to prescribe a wall friction F. Strictly this renders a one-dimensional model inexact, although for long thin samples, cross-sectional averaging will still lead to a one-dimensional model. Here we simply allow for side-wall friction by the addition of a friction term to the solid momentum equation. The equations describing the flow then take the form

$$\begin{aligned}
\rho_s(1-\phi)w_{tt} &= (1-\phi)\sigma_z + A + D - F, \\
\rho_f\phi v_t &= -\phi p_z - A - D, \\
(1-\phi)\sigma &= Ew_z - \alpha p, \\
A &= (1-\phi)C_{VM}\rho_f\left(v_t - w_{tt}\right), \\
D &= \frac{\eta_f\phi^2}{k}\left(v - w_t\right) + \frac{\rho_f c_F\phi^3}{\sqrt{k}}|v - w_t|\left(v - w_t\right), \\
\left(\rho_f\phi\right)_t + \left(\rho_f\phi v\right)_z &= 0, \\
\rho_f &= \rho_0\left(\frac{p}{p_0}\right)^{1/\gamma},
\end{aligned} \tag{3.19}$$

where

$$E = B + 2N, \quad \gamma = \frac{Mc_p}{Mc_p - R}, \tag{3.20}$$

and ρ_0 and p_0 are reference values of gas density and pressure. As before, subscripts t denote time derivatives, while subscripts z denote space derivatives. We suppose the wall friction term is given by

$$F = \frac{\mu_g(w - w_0)}{2\pi R d_g}, \tag{3.21}$$

where μ_g is the shear modulus of the glue, d_g is the glue thickness, R is the sample radius, and $w_0(z)$ is the initial displacement of the sample (this may be non-zero because we take as reference state the unstressed sample before it is pressurised).

The model is augmented by initial conditions

$$w_t = v = 0, \quad -\sigma = p = p_0 \quad \text{at} \quad t = 0. \tag{3.22}$$

Suitable boundary conditions are to prescribe solid and fluid stress at the surface, and zero displacement at the base, thus

$$\begin{aligned}
-\sigma = p = p_c \quad &\text{at} \quad z = l, \\
v = w = 0 \quad &\text{at} \quad z = 0.
\end{aligned} \tag{3.23}$$

The pressure in the chamber at the surface of the sample, p_c, is a function of time which decreases from its initial value p_0. The dynamics of this decrease depend on

the rate of escape of gas from the roof of the chamber. In fitting the experimental data, we use an exponential of the form

$$p_c = \exp(-t/t_c). \tag{3.24}$$

More general forms could be adopted, but (3.24) points out the importance of the chamber relaxation time scale t_c, which has an important part to play in the dynamics. Just as with a champagne cork, if the pressure decreases sufficiently slowly, the gas will be able to escape without fracturing the rock.

To describe the mechanism of fracture, we follow precepts first put forward in the context of soil mechanics. The total stress on the rock is the weighted sum of the stresses on rock grains and pore space, thus

$$\sigma_{\rm tot} = (1-\phi)\sigma - \phi p, \tag{3.25}$$

and the effective stress is

$$\sigma_{\rm eff} = \sigma_{\rm tot} + p = (1-\phi)(\sigma + p). \tag{3.26}$$

We hypothesize that fracturing occurs if the effective stress exceeds a yield stress $(1-\phi)\sigma_Y$, weighted by the solid volume fraction $(1-\phi)$, to indicate the dependence of yield on the number density of intergranular bonds. Fracturing of the sample thus occurs if

$$p + \sigma > \sigma_Y, \tag{3.27}$$

and in this case the boundary conditions in the fractures will be modified, as described later.

Non-dimensionalisation

We scale the variables as follows:

$$\begin{aligned} &\rho_f \sim \rho_0, \quad \sigma, p \sim p_0, \quad z \sim l, \quad t \sim t_0 = \frac{l}{v_0}, \quad w, w_0 \sim \bar{w} = \frac{p_0 l}{E}, \\ &v \sim v_0 = k^{1/4}\left(\frac{p_0}{\phi\rho_0 c_F l}\right)^{1/2}, \quad D \sim \frac{\phi p_0}{l}, \quad A \sim \frac{\rho_0 v_0^2}{l}, \end{aligned} \tag{3.28}$$

so that in dimensionless form (using the same letters to denote the dimensionless variables[1]), we have the dimensionless model

$$\begin{aligned} \varepsilon(1-\phi)w_{tt} &= (1-\phi)\sigma_z + \nu A + D - \lambda\left(w - w_0\right), \\ \nu\phi p^{1/\gamma} v_t &= -\phi p_z - \nu A - D, \\ (1-\phi)\sigma &= w_z - \alpha p, \\ A &= (1-\phi)C_{VM} p^{1/\gamma}\left(v_t - \delta w_{tt}\right), \\ D &= \frac{(v - \delta w_t)}{Re_p c_F} + \phi p^{1/\gamma}\left|v - \delta w_t\right|\left(v - \delta w_t\right), \\ \left(p^{1/\gamma}\right)_t + \left(p^{1/\gamma} v\right)_z &= 0, \end{aligned} \tag{3.29}$$

[1]The notation $z \sim l$, for example, is an abbreviation for the process of writing $z = lz^*$, substituting into the model, and then in the resulting dimensionless equations, omitting the asterisks on the starred variables.

where the dimensionless parameters are

$$\varepsilon = \frac{\rho_s v_0^2}{E}, \quad \nu = \frac{\rho_0 v_0^2}{p_0}, \quad \lambda = \frac{\mu_g l^2}{2\pi R d_g E},$$

$$\delta = \frac{p_0}{E}, \quad Re_p = \frac{\rho_0 v_0 \sqrt{k}}{\eta_f}; \tag{3.30}$$

α was defined in (3.5), and is presumed to be $O(1)$.

Symbol	Meaning	Typical value
c_F	Ergun coefficient	0.5
d_g	glue thickness	0.8 mm
E	elastic constant	10^{11} Pa
k	permeability	10^{-12} m^2
l	sample length	0.06 m
p_0	initial pressure	10 MPa
R	sample radius	1.2 cm
t_c	chamber relaxation time scale	1 ms
γ	specific heat ratio	1.4
η_f	gas viscosity	1.75×10^{-5} Pa s
μ_g	glue shear modulus	10^9 Pa
ρ_0	gas density	115 kg m^{-3}
ρ_s	solid density	2.6×10^3 kg m^{-3}
σ_Y	yield stress	2 MPa
ϕ	porosity	0.4

Table 1: Typical values of the physical parameters of the model. The gas properties are those of nitrogen at room temperature.

To estimate the values of these parameters, we use the values in table 1. From these, we compute the scales of the model, shown in table 2, and hence we compute typical values of the dimensionless parameters, as indicated in table 3.

Scale	Typical value
t_0	22 ms
v_0	2.7 m s^{-1}
$\bar{w}$	0.6×10^{-2} mm

Table 2: Typical values of the derived scales of the model.

The parameters ε, ν and δ are all small, and the Reynolds number Re_p is moderately large. We therefore neglect terms of order Re_p^{-1}, ν and δ, but retain temporarily the singular term εw_{tt}, which is instrumental in describing the elastic waves which

Parameter	Typical value
a	22
p^*	0.12
Re_p	17.7
δ	10^{-4}
ε	1.9×10^{-7}
λ	0.6
ν	0.8×10^{-4}

Table 3: Typical values of the derived parameters of the model.

might propagate through the sample. The resultant model reduces to

$$\begin{aligned} \varepsilon(1-\phi)w_{tt} &= w_{zz} - \beta p_z - \lambda\,(w - w_0)\,, \\ p_t^{1/\gamma} + \left(p^{1/\gamma} v\right)_z &= 0, \\ -p_z = p^{1/\gamma}|v|v, & \end{aligned} \tag{3.31}$$

where

$$\beta = \phi + \alpha, \tag{3.32}$$

and $\beta = O(1)$. By eliminating v, we find that the pore gas pressure satisfies the nonlinear diffusion equation

$$\frac{\partial p^{1/\gamma}}{\partial t} = \frac{\partial}{\partial z}\left(\left|\frac{p^{1/\gamma}}{p_z}\right|^{1/2} \frac{\partial p}{\partial z}\right). \tag{3.33}$$

This can also be written in terms of the scaled gas density $\rho = p^{1/\gamma}$, which provides the simpler equation for numerical purposes,

$$\frac{\partial \rho}{\partial t} = \frac{\partial}{\partial z}\left(\left|\frac{\gamma\rho^{\gamma}}{\rho_z}\right|^{1/2} \frac{\partial \rho}{\partial z}\right). \tag{3.34}$$

The dimensionless pressure in the chamber above the sample is also denoted as $p_c(t)$, and our choice of exponential in (3.24) yields the dimensionless form

$$p_c = \exp(-at), \tag{3.35}$$

where

$$a = \frac{t_0}{t_c} = \frac{l}{v_0 t_c}. \tag{3.36}$$

Initially, the sample is at rest, the chamber pressure $p_c = 1$ and this is also the initial pore pressure and solid stress through the sample. Up until the time when the sample lifts off the base, we take the solid displacement and gas flux to be zero at the base. At the surface of the sample, both solid stress and gas pressure equal the chamber

pressure. Thus suitable initial and boundary conditions for the sample displacement and gas pressure, up until fracture or lift off occurs, are

$$w = w_0 = -(1-\beta)z, \quad w_t = v = 0 \quad \text{at} \quad t = 0, \quad (\text{and } -\sigma = p = 1),$$

$$p_z = w = 0 \quad \text{at} \quad z = 0,$$

$$p = p_c, \quad w_z = -(1-\beta)p_c \quad \text{at} \quad z = 1. \tag{3.37}$$

The fracture criterion (3.27) can be written in the dimensionless form

$$w_z + (1-\beta)p > p^*, \tag{3.38}$$

where

$$p^* = \frac{(1-\phi)\sigma_Y}{p_0}. \tag{3.39}$$

The quantity $(1-\beta)$ represents the initial compressive displacement (at the surface) of the sample due to the imposition of the initial chamber pressure, with $\beta < 1$ representing a compression, and $\beta > 1$ representing inflation. Mainly for simplicity, we assume that $\beta = 1$, and in this case we have

$$w = w_0 = 0 \quad \text{at} \quad t = 0, \quad w_z = 0 \quad \text{at} \quad z = 1. \tag{3.40}$$

The relaxation and fracture parameters a and p^* are given in table 3; typically a is large and p^* is small. The consequences of these estimates are that diffusive relaxation of the pore gas pressure is relatively slow, and the fractures occur relatively close to each other in the sample. In the following sections we describe the nature of the solutions to these equations.

Primary fracture

The basic picture we have of what happens following release of the chamber pressure is as follows. The surface pressure at $z = 1$ decreases (over a time scale of $O(1/a)$), and as it does so the pore pressure profile p decreases also, propagating a wave down into the sample. At the same time, the solid stress relaxes quasi-statically, since the acceleration term is small. To get an indication of the behaviour of the solid displacement w, we can reason as follows. Neglecting ε and taking $\beta = 1$, $(3.31)_1$ implies

$$w_{zz} - p_z - \lambda w \approx 0, \tag{3.41}$$

representing force balance in the rock. At early times, the pore pressure has only changed near the surface, and its gradient with z is large; thus w_{zz} is larger than λw, so that approximately $w = \tilde{w}$, where

$$\tilde{w}_z = p - p_c, \quad \tilde{w} = \int_0^z (p - p_c)\, dz. \tag{3.42}$$

Consulting (3.42), we see that $\tilde{w}_z$ is a monotonically decreasing function of z, and thus the fracture criterion (3.38) is first satisfied at the base $z = 0$ when $p - p_c > p^*$.

In particular, without glue (when $\lambda = 0$), the model predicts initial lift off at the sample base.

An approximate correction to (3.42) at early times, or when λ is small, is given by

$$w_z \approx p - p_c - \lambda \int_z^1 \tilde{w}\, dz \tag{3.43}$$

representing the solid strain in the rock. Since $\tilde{w}$ is a monotonically increasing function of z, we see that w_z increases with z near the base (where $p_z \approx 0$) and then decreases near the surface (where p_z is large). Thus w_z reaches p^* first at an interior point below the surface, as observed.

Attenuation

In the above description, we have assumed a quasi-static elastic response of the sample based on the small value of ε. At closer inspection, this seems risky, since the general solution of $(3.31)_1$, given p_z, will be the sum of the particular quasi-static solution, together with a pair of high speed elastic waves which propagate up and down the sample. The consequent rapid fluctuations in w might then be expected to lead to rapid disintegration of the sample without the ordered top-down sequence which is observed. In fact, so long as the surface pressure decreases over a time scale greater than $O(\sqrt{\varepsilon})$, thus explicitly if

$$a\sqrt{\varepsilon} \ll 1, \tag{3.44}$$

we can see that the quasi-static displacement profile not only satisfies the boundary conditions, but also the initial conditions. A simple analogous problem is the forced oscillator equation

$$\varepsilon \ddot{w} + w = R(t), \tag{3.45}$$

where it is known (Fowler and Kember 1996) that the slowly varying solution $w \sim R(t)$ is accompanied by free oscillations $\propto \exp(\pm it/\sqrt{\varepsilon})$ of exponentially small amplitude. On this basis, we expect the accompanying elastic waves here to have negligible amplitude. This conclusion would not be true if the surface pressure were ramped down instantaneously (or very rapidly). Attenuation is present in the model through the terms of $O(\nu)$ and $O(\delta)$, but is not operative over the short time scales of the experiment.

Explosion

Once an initial fracture has formed, either in the interior or at the base of the sample, the separated block can lift off. In this second phase of the motion, we suppose that the glue is also fractured, so that there is no longer any resistive traction at the walls. After separation, the gas flow within the separated blocks is still described by the previous model equations, but we must now consider the evolution of the crack widths. In addition, we address the issue of secondary fragmentation within the separated blocks. Suppose during the experiment we have a sequence of fractures formed at $z_1, z_2, \ldots$, where the fracture at z_i opens into a crack whose upper and lower

surfaces are denoted z_i^+, z_i^-. The (dimensional) gas flux into the crack is $\phi(v-w_t)$, and therefore conservation of gas mass in the i-th crack yields the dimensional equation

$$\frac{d}{dt}\left[\rho_i\left(z_i^+ - z_i^-\right)\right] = -\left[\rho_i\phi\left(v - w_t\right)\right]_-^+, \tag{3.46}$$

where ρ_i is the gas density in the i-th crack. This equation determines the gas density, and thus the pressure, in the crack.

To render the equation dimensionless, we scale the variables as before, and in addition we scale the crack boundaries as

$$z_i^\pm \sim l; \tag{3.47}$$

this leads to the dimensionless form of (3.46),

$$\frac{d}{dt}\left[\rho_i\left(z_i^+ - z_i^-\right)\right] = -\left[\rho_i\phi\left(v - \delta w_t\right)\right]_-^+, \tag{3.48}$$

where $\rho_i = p_i^{1/\gamma}$.

In the i-th block (z_i^+, z_{i+1}^-), it is appropriate to put

$$w = \frac{z_i^+}{\delta} + W \tag{3.49}$$

(i. e., the displacement is relative to the base of the block), and then the crack width equation (3.48) becomes

$$\frac{d}{dt}\left[\rho_i\left(z_i^+ - z_i^-\right)\right] = -\left[\rho_i\phi\left(v - \dot{z}_i - \delta W_t\right)\right]_-^+, \tag{3.50}$$

bearing in mind that we may take $\dot{z}_i^+ = \dot{z}_{i+1}^-$. In addition, the momentum equation $(3.31)_1$ can be written

$$\frac{\varepsilon}{\delta}(1-\phi)\ddot{z}_i^+ + \varepsilon(1-\phi)W_{tt} = (1-\phi)\sigma_z - \phi p_z. \tag{3.51}$$

Ignoring the displacement acceleration term (but not the block acceleration term), and bearing in mind that the total stress $\sigma_{\rm tot} = (1-\phi)\sigma - \phi p = -p_i$ at the i-th crack, we see that integration of (3.51) over the block leads to the approximate block acceleration equation

$$\frac{\varepsilon}{\delta}(1-\phi)l_i\ddot{z}_i^+ \approx p_i - p_{i+1}, \tag{3.52}$$

where $l_i = z_{i+1}^- - z_i^+$ is the (constant) length of the i-th block. If the i-th fracture forms at $z = z_i$ at time $t = t_i$, then the initial conditions for (3.52) are

$$z_i^+ = z_i, \quad \dot{z}_i^+ = 0 \quad \text{at} \quad t = t_i. \tag{3.53}$$

In summary, the gas pore pressure in the blocks continues to satisfy (3.33), with the boundary conditions that

$$p = p_i \quad \text{at} \quad z = z_i^+, \quad p = p_{i+1} \quad \text{at} \quad z = z_{i+1}^-. \tag{3.54}$$

The crack pressures are determined by solving (3.50), which takes the approximate form

$$[z_i]_-^+ \frac{d}{dt}\left(p_i^{1/\gamma}\right) = \left[\phi\left|\frac{p^{1/\gamma}}{p_z}\right|^{1/2} p_z - (1-\phi)p_i^{1/\gamma}\dot{z}_i\right]_-^+, \tag{3.55}$$

and the block motion is determined by solving (3.52).

When the fracture criterion (3.27) is written dimensionlessly, it becomes

$$(1-\phi)(\sigma+p) > p^*; \tag{3.56}$$

this is identical to (3.38), but the form above is more useful within the blocks. Since in the blocks we have, from (3.51),

$$(1-\phi)\sigma - \phi p + p_i \approx \frac{\varepsilon}{\delta}(1-\phi)\ddot{z}_i^+\left(z - z_i^+\right) = (p_i - p_{i+1})\left(\frac{z-z_i^+}{l_i}\right), \tag{3.57}$$

the criterion for secondary fracture within the blocks is simply

$$p - \bar{p}(z) > p^*, \tag{3.58}$$

where

$$\bar{p}(z) = p_{i+1}\left(\frac{z-z_i^+}{l_i}\right) + p_i\left\{1 - \left(\frac{z-z_i^+}{l_i}\right)\right\} \tag{3.59}$$

is the linear profile joining the pressures at the top and bottom of the block.

When an internal fracture is generated at z_i, then $p_i > p_{i+1}$, and, since $\varepsilon/\delta \sim 10^{-3}$, the block accelerates rapidly upwards. As it does so the crack pressure decreases according to (3.55), and we surmise that p_i rapidly approaches p_{i+1}, and the block speed reaches a constant, as is observed in the experiments.

The physical mechanism for this relaxation is akin to that of the removal of a piston from a tube. The necessity to fill the expanding void in the crack causes an effective suction which acts as a drag on the ascending block. Mathematically, we can provide some insight into this by consideration of (3.55). Considering for simplicity the case of the first fracture, where $i = 1$, z_1^- is constant, and $p_{i+1} = p_c$ is prescribed, we may write (3.55) in the form

$$\frac{d}{dt}\left[z_1^{1-\phi} p_1^{1/\gamma}\right] = \frac{\phi f}{z_1^{\phi}}, \tag{3.60}$$

where f is the porous gas flux from the adjacent blocks into the expanding crack. A simple idea of how f depends on the crack pressure p_1 follows from elementary consideration of the way in which diffusion operates in the rock. As p_1 reduces, the flux to the crack will increase, thus $\dfrac{\partial f}{\partial p_1} < 0$. (Of course it is more complicated than this: f will also decrease with time, as the diffusive boundary layers grow into the blocks.) Assuming this, then (3.52) suggests $\dfrac{\partial f}{\partial \ddot{z}_1} < 0$. Blithely ignoring exponents and other detail, the structure of (3.60) is thus

$$\frac{d}{dt}\left[z_1 p_1\right] \sim -\ddot{z}_1, \tag{3.61}$$

whence, loosely,

$$z_1 p_1 \sim A - \dot{z}_1, \tag{3.62}$$

and substituting back into (3.52) yields

$$\frac{\varepsilon}{\delta}(1-\phi) l_1 z_1 \ddot{z}_1 \sim A - \dot{z}_1 - p_c, \tag{3.63}$$

which would indicate a damped, possibly oscillatory, approach to the equilibrium where $p_1 = p_c$. This damping is found in our numerical results, as well as being implicit in the experimental results.

After (rapid) equilibration, $p_i \approx p_{i+1}$, and the crack pressures will all decrease with the surface pressure p_c. Further internal fractures in the blocks may then occur, according to (3.58) and (3.59), if $p - p_c > p^*$, while fracture in the lowest (attached) block mimics the initial primary fracture.

4 Numerical results

Equations (3.33) and (3.41) together with the associated initial and boundary conditions have been solved numerically using Matlab to determine the solid displacement w and gas pore pressure p. The gas diffusion equation (written as (3.34) for the density) was solved using small time steps and the `pdepe` solver for a glued-down sample of rock, and the boundary value problem (3.41) for w in the glued-in piece was solved for by using a Green's function approach. Then the fragmentation criterion was checked at each time step.

After fragmentation had occurred, the equations (3.52) and (3.55) for the evolution of gap size and pressure were solved using the Runge-Kutta `ode45` solver, again with small time steps, and the gas fluxes from adjacent rock segments were calculated as required by `ode45`. The process was continued, checking for further fracture in every piece of rock at every time step, and increasing the number of coupled differential equations to be solved each time a new break was detected.

Parameter values are essentially as given in table 1, but with slightly different values of ϕ and σ_Y, as noted in the caption to figure 4. The value of ϕ is that appropriate for the experimental data in figure 3.

Figure 4 shows the evolution with time using snapshots of the gas pore pressure p and the solid compressive stress $-\sigma$. As the surface pressure at 60 mm lowers, a diffusive boundary layer profile (solid line) of the gas pressure migrates into the column. The compressive stress in the solid responds quasi-statically, and according to (3.29) and (3.43), is given (approximately, if λ is small) by

$$p_c + \sigma \approx \frac{\phi}{1-\phi}\,(p - p_c)\,; \tag{4.1}$$

since $\dfrac{\phi}{1-\phi} \approx 1$, this can be seen in the first panel in figure 4. The slight minimum in the solid stress is due to the non-zero value of λ. Consequently, fracture first occurs near this minimum, as shown in the second panel, where, immediately following

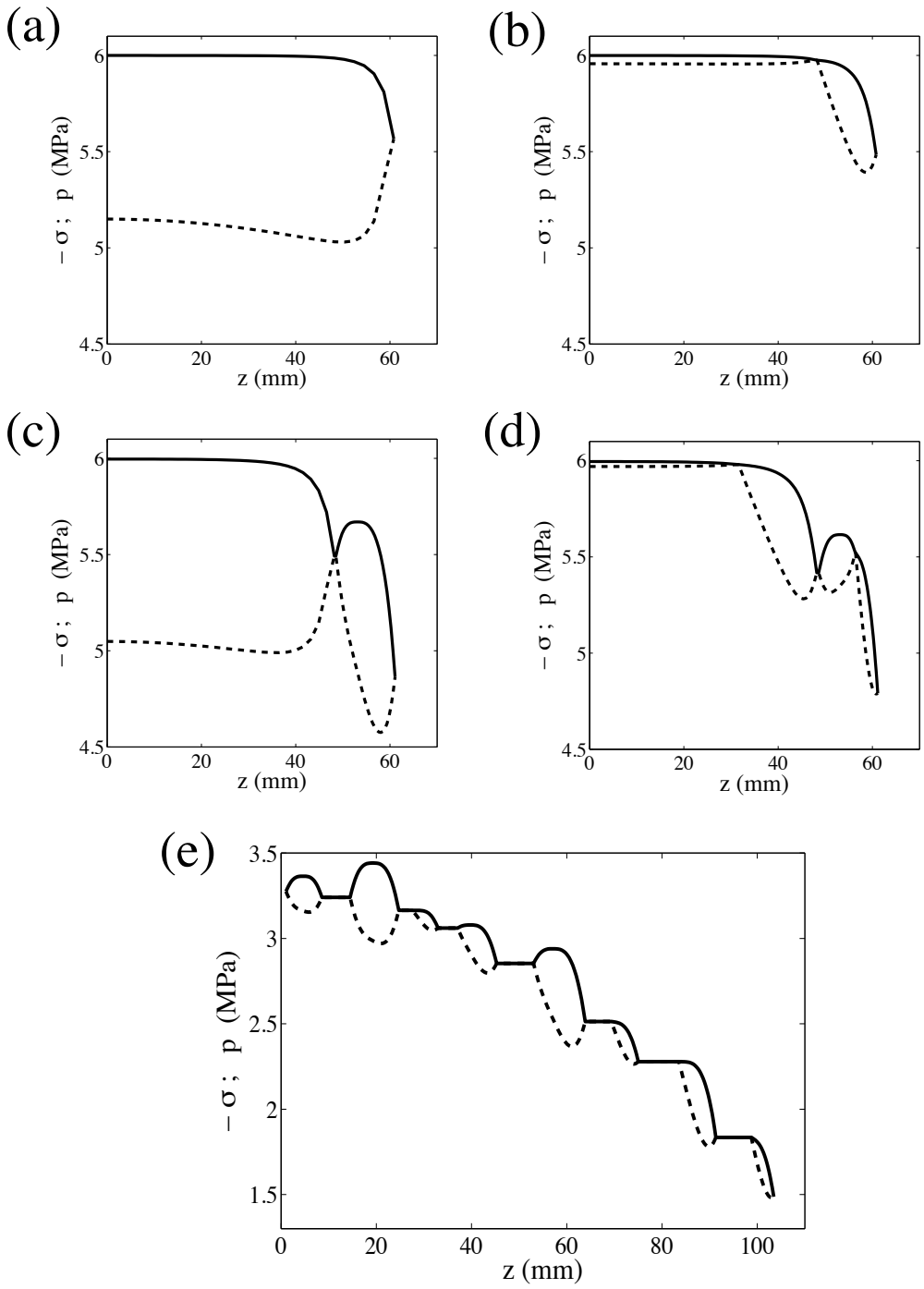

Figure 4: Gas pore pressure p (solid lines) and solid compression $-\sigma$ (dashed lines). (a) $t = 0.07$ ms: just before the first fracture at $t = 0.08$ ms, $z = 48$ mm, when $p - (-\sigma) = \sigma_Y$; (b) $t = 0.085$ ms: just after the first fracture; (c) $t = 0.205$ ms: just before the second fracturing event at $t = 0.215$ ms, when both a primary and a secondary fragmentation occur in the same time step at $z = 31$ and 55 mm respectively; (d) $t = 0.220$ ms: just after this double fragmentation event; (e) $t = 1.39$ ms: after multiple primary, secondary and liftoff fragmentations. Note the different scales on the final plot, reflecting the overall lowering of pressures after so much time, and the level regions which are the expanding gas-filled gaps between ejected rock fragments. Parameter values used in solving (3.33) and (3.41) are those in Table 1, with the exceptions that $\sigma_Y = 1$ MPa, $p_0 = 6$ MPa, and $\phi = 0.48$, the latter two chosen to reflect known quantities in the experimental results of figures 2 and 3. In addition we have taken $\beta = 1$. The corresponding values of t_0 and p^* are $t_0 = 32.2$ ms and $p^* = 0.087$.

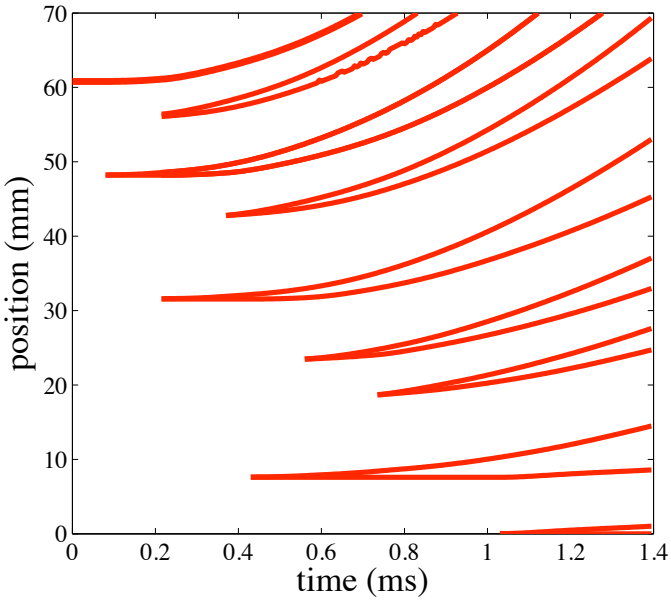

Figure 5: Primary and secondary fractures in the simulation corresponding to figure 4. This figure can be compared with figure 3.

fracture, the solid stress in the basal part of the column relaxes rapidly towards the gas pore pressure, which is still aproximately p_c. Continued diffusion of the gas pressure draws down the pressure in the ejected block, while the pressure and stress profiles in the basal column repeat their evolution as in panel one. This process repeats itself, as indicated in panels four and five, causing a sequence of fractures and consequent ejection of the blocks. Figure 5 shows the consequent pattern of fractures, plotted similarly to figure 3, to which it can be (favourably) compared.

5 Discussion

In our model, fragmentation is largely controlled by two quantities. The first of these is the yield stress σ_Y. As indicated by (3.39), if this is less than the initial confining pressure, then fragmentation is likely, providing the contained gas cannot escape sufficiently rapidly. In the experiment, the time scale for gas escape is t_0, and this is determined through the gas pore velocity scale v_0, defined in (3.28). Thus for low permeability, v_0 is low, t_0 is high, and in this case fragmentation is likely to occur.

While our model is designed to simulate the fragmentation experiments, which are themselves designed to provide insight into explosive volcanic eruptions, it is less easy to draw theoretical conclusions which can be applied to volcanic processes. In the experiment, the rock is already vesicular and porous when depressurisation commences.

However, this might not always be the case in volcanic eruptions. At an eruption,

the sudden depressurisation by the removal of an overburden or volcanic plug can cause volatile exsolution to a very different extent, depending on the amount of depressurisation and on magma properties such as viscosity, diffusivity and volatile disequilibrium. For instance, at sustained Plinian-type eruptions an equilibrium can be assumed between magma ascent and depressurisation-driven volatile exsolution. This results in a highly vesicular magma; consequently, magma disintegration (fragmentation) can occur, if the stresses generated in the melt phase by the vesiculation-driven expansion exceed the yield strength of the magma.

A completely different picture can be drawn for the typically short-lived Vulcanian-style eruptions. Here the erupting magma is commonly highly viscous and, given the usually short time scale between plug removal and the consequent initiation of sudden depressurisation and explosive ejection of the magma, minor additional volatile exsolution driven by the rapid depressurisation will occur. The laboratory experiments described and modelled here bear most resemblance to the latter eruption style. Still, details of the fracturing process in the volcanic situation are assumed to be somewhat different to that in the experiment, and the details of the model will thus also be necessarily different.

Even if we restrict our attention to the present experiment, there are issues in our model which are at least questionable. The precise form of the interphasic drag terms used in (3.16) are based on experimental results obtained under steady equations. In the present case, it is likely that inertial effects may be important (Chojnicki *et al.* 2006), and if, for example, we introduced an inertial term proportional to $\dfrac{\partial \mathbf{V}}{\partial t}$ into (3.16), the resulting model (3.33) for p would become hyperbolic rather than parabolic. It seems unlikely that this would substantially alter the results, however.

The wall friction term (3.21) was introduced into the model because without it, the model always predicted initial lift off at the base of the column. And indeed, this is what is seen, since if the rock is not glued in place, then indeed basal lift-off occurs first. Initial efforts to model the effect of the wall glue used a viscous formulation, but it is thought that the elastic form better suits the resistance prior to rupture. That is to say, once the rock ruptures, the glue, having less strength, ruptures also, and offers no further resistance. We have chosen a value of the glue shear modulus indicating its weaker strength, and comparable to typical values for polymer glues.

An issue of interest concerns the robustness of the results we have obtained. Although more detailed explorations will be conducted in future work, we can state that the model fits the experimental results both qualitatively and quantitatively without the need for special choices of parameters. The results obtained depend in their quantitative predictions on the choice of the parameters β, λ, p^* and a. While values of β and λ are open to doubt, the choices presented here were in fact our original choices. The same applies to the choice of yield stress σ_Y. Variation of these parameters does vary the results, but not to any marked degree.

6 Conclusions

We have constructed a mathematical model of the fragmentation process in the experiments described by Spieler *et al.* (2004). In our model, the rock is elastic and subject to a fracture criterion which depends on the local effective tensile stress in the rock. Following a fracture, the ejected fragment is expelled by the acceleration applied by the higher gas pressure below the fragment. However, the expulsion of the fragment and consequent widening of the fracture beneath requires that the pore gas be sucked from the fragment to fill the expanding fracture, and this suction causes a deceleration of the ejected fragment. Because the gas depressurisation wave propagates relatively slowly, the effective tensile stress reaches a maximum at a finite depth in the sample, and thus fracturing occurs first at finite depth. As each fragment is ejected, the crack pressure rapidly decreases towards the surface pressure, and the process is repeated. In addition, secondary fracture can occur within the ejected samples.

All of this behaviour is seen in the laboratory experiment, and our numerical solutions of the model indicate good qualitative and quantitative agreement with the experiments. In future work we will explore in more detail how the numerical results compare to the range of experimental results, and in particular whether some simple rules of thumb, for example concerning fracture threshold porosity, can be deduced from the model, and we will also explore whether yet simpler representations of the model solutions can be found in certain parameter régimes.

Acknowledgements

We acknowledge the support of the Mathematics Applications Consortium for Science and Industry (`www.macsi.ul.ie`) funded by the Science Foundation Ireland mathematics initiative grant 06/MI/005. The experimental work was funded by the Japan Society for the Promotion of Science (no. P05–318). We are thankful to Mie Ichihara for her help building the laboratory as well as for useful discussions. Further we thank Kei Kurita for sharing the high-speed camera with us. We also thank Peter Howell for his customary illuminating insights.

References

Alidibirov, M. 1994 A model for viscous magma fragmentation during volcanic blasts. Bull. Volcanol. **56**, 459–465.

Alidibirov, M. and D. B. Dingwell 1996 Magma fragmentation by rapid decompression. Nature **380**, 146–148.

Alidibirov, M. and D. B. Dingwell 2000 Three fragmentation mechanisms for highly viscous magma under rapid decompression. J. Volcanol. Geotherm. Res. **100**, 413–421.

Biot, M. A. 1956 Theory of propagation of elastic waves in a fluid-saturated porous solid. I. Low-frequency range. J. Acoust. Soc. Amer. **28**, 168–178.

Biot, M. A. 1962 Mechanics of deformation and acoustic propagation in porous media. J. Appl. Phys. **33**, 1,482–1,498.

Cashman, K. V., B. Sturtevant, P. Papale and O. Navon 2000 Magmatic fragmentation. In: Encyclopedia of volcanoes, ed. H. Sigurdsson. Academic Press, San Diego, pp. 421–430.

Chojnicki, K., A. B. Clarke and J. C. Phillips 2006 A shock-tube investigation of the dynamics of gas-particle mixtures: implications for explosive volcanic eruptions. Geophys. Res. Letts. **33**, L15309, doi:10.1029/2006GL026414.

Dingwell, D. B. 1996 Volcanic dilemma: flow or blow? Science **273**, 1054–1055.

Dingwell, D. B. 2006 Transport properties of magmas: diffusion and rheology. Elements **2**, 281–286.

Dingwell, D. B. and S. L. Webb 1989 Structural relaxations in silicate melts and non-newtonian melt rheology in geologic processes. Phys. Chem. Miner. **16**, 508–516.

Fowler, A. C. and G. Kember 1996 On the Lorenz-Krishnamurthy slow manifold. J. Atmos. Sci. **53**, 1433–1437.

Gilbert, J. S. and R. S. J. Sparks (eds.) 1998 The physics of explosive volcanic eruptions. Geological Society Special Publication no. 145. Geological Society, London.

Ichihara, M., D. Rittel and B. Sturtevant 2002 Fragmentation of a porous viscoelastic material: Implications to magma fragmentation, J. Geophys. Res. **107** (B10), 2229, doi:10.1029/2001JB000591.

Kennedy, B., O. Spieler, B. Scheu, U. Kueppers, J. Taddeucci and D. B. Dingwell 2005 Conduit implosion during Vulcanian eruptions. Geology **33**, 581–584.

Koyaguchi, T. and N. K. Mitani 2005 A theoretical model for fragmentation of viscous bubbly magmas in shock tubes. J. Geophys. Res. **110** (B10), B10202, doi:10.1029/2004JB003513.

Koyaguchi, T., B. Scheu, N. K. Mitani and O. Melnik 2008 A fragmentation criterion for highly viscous bubbly magmas estimated from shock tube experiments. J. Volcanol. Geotherm. Res. **178**, 58–71.

McBirney, A. R. and T. Murase 1970 Factors governing the formation of pyroclastic rocks. Bull. Volcanol. **34**, 372–384.

Melnik, O. 2000 Dynamics of two-phase conduit flow of high-viscosity gas-saturated magma: large variations of sustained explosive eruption intensity. Bull. Volcanol. **62**, 153–170.

Namiki, A. and M. Manga 2005 Response of a bubble bearing viscoelastic fluid to rapid decompression: implications for explosive volcanic eruptions. Earth Planet. Sci. Letts. **236**, 269–284.

Nield, D. A. and A. Bejan 2006 Convection in porous media, 3rd ed. Springer, New York.

Papale, P. 1999 Strain-induced magma fragmentation in explosive eruptions. Nature **397**, 425–428.

Papale, P., A. Neri and G. Macedonio 1998 The role of magma composition and water content in explosive eruptions. I. Conduit ascent dynamics. J. Volcanol. Geotherm. Res. **87**, 75–93.

Robinson, M., A. C. Fowler, A. J. Alexander and S. G. B. O'Brien 2008 Waves in Guinness. Phys. Fluids **20**, 067101.

Scheu, B., M. Ichihara, O. Spieler and D. B. Dingwell 2008a A closer look at magmatic fragmentation. Geophys. Res. Abstracts, **10**, EGU2008-A-04786.

Scheu, B., U. Kueppers, S. Mueller, O. Spieler and D. B. Dingwell 2008b Experimental volcanology on eruptive products of Unzen volcano. J. Volcanol. Geotherm. Res. **175**, 110–119.

Scheu, B., O. Spieler and D. B. Dingwell 2006 Dynamics of explosive volcanism at Unzen volcano: an experimental contribution. Bull. Volcanol. **69**, 175–187.

Sparks, R. S. J. 1978 The dynamics of bubble formation and growth in magmas: a review and analysis. J. Volcanol. Geotherm. Res. **3**, 1–37.

Spieler, O., B. Kennedy, U. Kueppers, D. B. Dingwell, B. Scheu and J. Taddeucci 2004 The fragmentation threshold of pyroclastic rocks. Earth Planet. Sci. Letts. **226**, 139–148.

Verhoogen, J. 1951 Mechanics of ash formation. Amer. J. Sci. **249**, 729–739.

Zhang, Y. X. 1999 A criterion for the fragmentation of bubbly magma based on brittle failure theory. Nature **402**, 648–650.